Necrotic upper tips1 mimics heat and drought stress and encodes a protoxylem-specific transcription factor in maize

Zhaobin Dong[a,1] ⓘ, Zhennan Xu[b,1], Ling Xu[a,1], Mary Galli[b], Andrea Gallavotti[b] ⓘ, Hugo K. Dooner[b,2], and George Chuck[a,2]

[a]Plant Gene Expression Center, University of California Berkeley, Albany, CA 94710; and [b]Waksman Institute, Rutgers University, Piscataway, NJ 08854

Maintaining sufficient water transport during flowering is essential for proper organ growth, fertilization, and yield. Water deficits that coincide with flowering result in leaf wilting, necrosis, tassel browning, and sterility, a stress condition known as "tassel blasting." We identified a mutant, *necrotic upper tips1* (*nut1*), that mimics tassel blasting and drought stress and reveals the genetic mechanisms underlying these processes. The *nut1* phenotype is evident only after the floral transition, and the mutants have difficulty moving water as shown by dye uptake and movement assays. These defects are correlated with reduced protoxylem vessel thickness that indirectly affects metaxylem cell wall integrity and function in the mutant. *nut1* is caused by an *Ac* transposon insertion into the coding region of a unique *NAC* transcription factor within the *VND* clade of *Arabidopsis*. NUT1 localizes to the developing protoxylem of root, stem, and leaf sheath, but not metaxylem, and its expression is induced by flowering. NUT1 downstream target genes function in cell wall biosynthesis, apoptosis, and maintenance of xylem cell wall thickness and strength. These results show that maintaining protoxylem vessel integrity during periods of high water movement requires the expression of specialized, dynamically regulated transcription factors within the vasculature.

maize | vasculature | protoxylem | water transport | flowering

Plant fertilization and seed set require optimal environmental conditions, including adequate water supply and moderate ambient temperatures. During flowering, maize male florets must be properly hydrated in order for the lodicules to expand, open the spikelets, and allow pollen to shed. In addition, optimal water levels are required to allow growth and elongation of the female carpels, or silks, which are the extremely water rich floral organs. Because the majority of cultivated maize is rain irrigated, this crop is acutely vulnerable to climatic change. Under water deficits, pollen shedding is inhibited, silk elongation stops, and fertilization does not occur efficiently, leading to severe yield loss (1). In addition, when temperatures reach over 35 °C, the male inflorescence of maize, the tassel, experiences heat stress that negatively impacts maize pollen fertility (2). When subjected to excessive heat, maize plants develop a syndrome known as "tassel blasting," where male floral organs desiccate and brown, and the pollen becomes infertile, preventing fertilization and dramatically reducing yield. Separating heat and drought stress phenotypes can be difficult because under field conditions both stresses often go together. However, both stresses have separable effects on a very wide range of basic plant processes in maize, including photosynthetic rate, transpiration rate, levels of reactive oxygen species, and stomatal conductance (3), although they both also function synergistically. Tassel blasting in maize refers strictly to a type of heat stress phenotype found in the male inflorescence and can even occur in fully hydrated plants, while drought stress causes a wide range of separate whole plant phenotypes (4). Due to rapidly changing climatic patterns,

potential maize yield losses from frequent drought and heat stress conditions may reach up to 12% a year (5). Thus, uncovering the genetic pathways underlying tassel blasting and drought stress has critical importance.

In the field, ambient water levels are constantly changing, and the plant must adapt and adjust to fluctuations such as drought. One major consequence of drought stress is the creation of water vapor bubbles within the vessels, or cavitations, that can ultimately disrupt the water column (6). In maize, acoustic measurements of growing maize plants demonstrated that more than half of all vascular bundles cavitate depending on time of day and environmental conditions (7). In severe cases, cavitation may lead to embolisms that block water movement. For example, at midday when xylem tension is highest, up to 70% of all large metaxylem vessels in maize were observed to have embolisms (8) that may severely reduce hydraulic conductivity. Embolized xylem vessels in maize can be repaired, and the water column restored due to radial water movement from adjacent cells, including the protoxylem (9). This functional relationship, however, implies that hydraulic connectivity must exist between the metaxylem and the protoxylem, although the exact path for water between these cells is unknown. In other plants, embolism repair is thought to occur at night when transpiration ceases and pressure within the xylem switches from negative to positive (7).

Significance

When water deficits coincide with flowering in maize they result in severe developmental consequences such as leaf wilting, tassel browning, and sterility, a condition known as "tassel blasting." Due to global warming, tassel blasting is becoming a major problem that can greatly reduce yields. *Necrotic upper tips1* (*nut1*) is a transcription factor that mimics tassel blasting when mutated. We show that NUT1 protein localizes to the developing protoxylem where it activates genes necessary for reinforcing the secondary cell wall, and thus enables these cells to withstand the high negative pressures required for long-distance water movement. Thus, *nut1* or its targets may be promising breeding targets to help maize resist the effects of rising temperatures in the future.

On a molecular level, drought stress also leads to increases in cellular abscisic acid (ABA) levels, and as a consequence, the formation of extra xylem (10). This phenomenon is mediated through noncell autonomous miR165 microRNA transport to vasculature in response to ABA (10).

Internal water levels also fluctuate across developmental phases, especially flowering (1), suggesting that vascular differentiation and function is dynamic throughout development. Indeed, direct measurements of xylem pressure in each mature maize leaf from the bottom of the plant to the top showed progressive increases in tension (11), especially in florally induced leaves. Because vasculature from leaves farther up the plant are under greater tension, associated xylem elements might require thicker, or stronger secondary cell walls in response, as observed in histological comparisons of maize juvenile and adult leaves (12, 13), and measurements of overall lignin and hemicellulose levels in other grasses (14). Furthermore, monocot xylem cells display morphological specialization depending on timing of initiation and the identity of the organs in which they are found (15). Ontogenetic changes in vascular development during different phases of growth have not been described in crop plants until only recently (16) and revealed that genes responsible for vascular maturation can be induced by the floral signal. Despite this, the molecular mechanism linking flowering to vascular development and changes in cell wall function is unknown.

NAC transcription factors have recently emerged as master regulators of xylem differentiation in *Arabidopsis* (17), and several members comprise a subfamily called the *VASCULAR-RELATED NAC-DOMAIN* (*VND*) genes. Originally identified from in vitro tracheary element culture experiments (18), seven of these genes are capable of conferring xylem cell identity when overexpressed (19), including *VND5*, *VND6*, and *NST1*. Interestingly, loss-of-function mutants in any of these genes have not been reported to confer obvious xylem mutant phenotypes or associate with water stress phenotypes, indicating a high level of functional redundancy. Despite this, *VND7* alone may be critical for xylem differentiation as gain-of-function experiments show that it functions in a forward feedback loop that specifies xylem identity (20), while acting as a bistable switch capable of inducing protoxylem differentiation when expressed above a critical threshold (21). A protein–DNA interaction network for *VND7*

has been reported, showing that the gene is induced by salt stress, sits downstream of the *E2Fc* gene network, and functions in combination with *VND6* and *PHV* to activate a range of secondary cell wall genes (20). Finally, *VND7* may exhibit functional diversity, and play a role in the differentiation of a wide range of xylem vessels, including both protoxylem, metaxylem, as well as fibers in several different tissues (22).

Only a few maize genes that play putative roles in conferring drought and heat stress resistance have been identified in maize through genome-wide association (GWAS) studies. For example, a GWAS survey of maize drought tolerance uncovered a vacuolar pyrophosphatase called *ZmVPP1* (23) that may function to enhance photosynthetic efficiency and root development. In addition, drought sensitivity within several maize lines is associated with the presence of a transposon insertion in the promoter of a *NAC* gene, *ZmNAC111* (24), though it is not a member of the *VND* clade. In tomatoes, overexpression of the *JUNG-BRUNNEN1 NAC* gene enhances drought tolerance (25), though this may be a result of altered hormone balance (26) as opposed to any direct effect on vascular development. In sum, although several *NAC* genes respond to a range of stress conditions and are known to function as transcription factors that control vascular development (19), none have been found to be involved in mediating heat stress, and any genetic connections between heat and drought stress responses remain unclear.

Here we identify a tissue-specific NAC gene called *necrotic upper tips1* (*nut1*) that mimics drought stress and tassel blasting and is required to fortify the secondary cell walls of the early forming protoxylem. *nut1* is induced during the adult/flowering phase of development in protoxylem, and when this gene is lost, the plants suffer both heat and drought stress phenotypes, indicating that these stresses share a common physiological mechanism. These results show that vascular transcription factors display temporal as well as tissue specificity in order to allow crop plants to cope with changing water demands. Thus, the *nut1* gene and its associated genetic pathway may be important tools with which to engineer crop plants to resist heat and drought stresses in the future.

Results

The *nut1* Mutant Causes Water Movement Defects during Flowering.

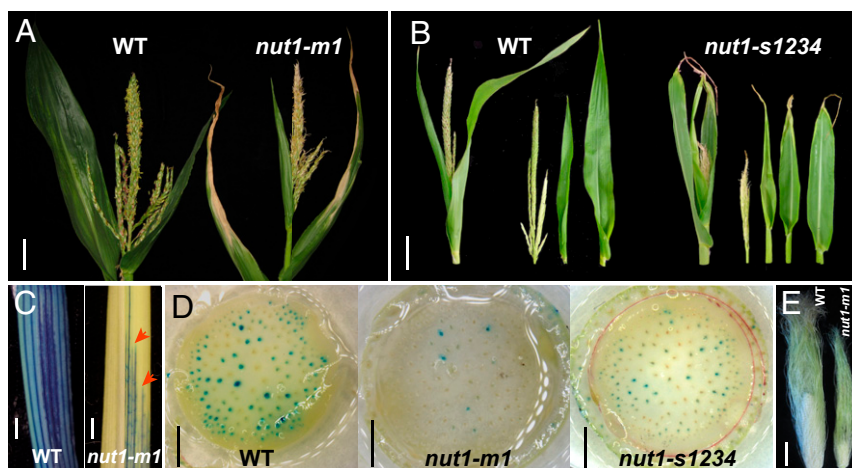The recessive *nut1-m1* mutant was isolated from an *Activator*

Fig. 1. The phenotype of the *nut1* mutant. (*A*) The *nut1-m1* mutant (*Right*) shows wilted necrotic leaf tips and a blasted tassel compared to wild type (WT, *Left*). (*B*) Comparison of uppermost leaves enclosing the tassel of WT versus a second allele *nut1-1234* mutant. Leaves on the *Right* were separated from each apex shown on the *Left*. Dye uptake and movement assay using sheaths (*C*) and floral stems (*D*). Red arrows indicate blockages in *nut1*. (*D*) Transverse floral stem sections taken at the same distance (1 cm) above the dye level. Dye uptake in *nut1* vascular bundles is reduced in stems of both alleles, indicating defective water transport. (*E*) *nut1* ear length and silk elongation are greatly reduced. (Scale bar, 5 cm in *A*, *B*, and *E* and 2 mm in *C* and *D*.)

Dong et al.

www.manaraa.com

(*Ac*) transposon screen (27). The mutant's drought and heat stress phenotypes were typically found only at the top of the plant, including wilted leaves, brown leaf tips, and a mostly sterile blasted tassel (Fig. 1*A*), despite being well watered. The leaf phenotypes only occur in the uppermost three to four nodes and are more pronounced at organ tips that often show necrosis. Similarly, the phenotype in the tassel tends to be more severe at the tips of the main spike and branches, displaying tassel blasting and partial sterility. These phenotypes are evident only after flowering, and mutants appear normal preflowering. A second allele, *nut1-s1234*, was isolated from an *Ac* excision event from the original *nut1-m1* stock. *nut1-s1234* shows identical leaf and tassel defects to *nut1-m1* (Fig. 1*B*). In addition, flowering plants of both *nut1* alleles display thinner stems, with fewer vascular bundles within floral nodes. A comparison of the cross-sectional areas and associated vascular bundle number in *nut1* compared to wild type indicates that vascular density is actually increased in the mutant (*SI Appendix*, Fig. S1), indicating that reduced vein number is not the direct cause of the phenotype. To elucidate if the wilting phenotype in *nut1* is caused by a water transport
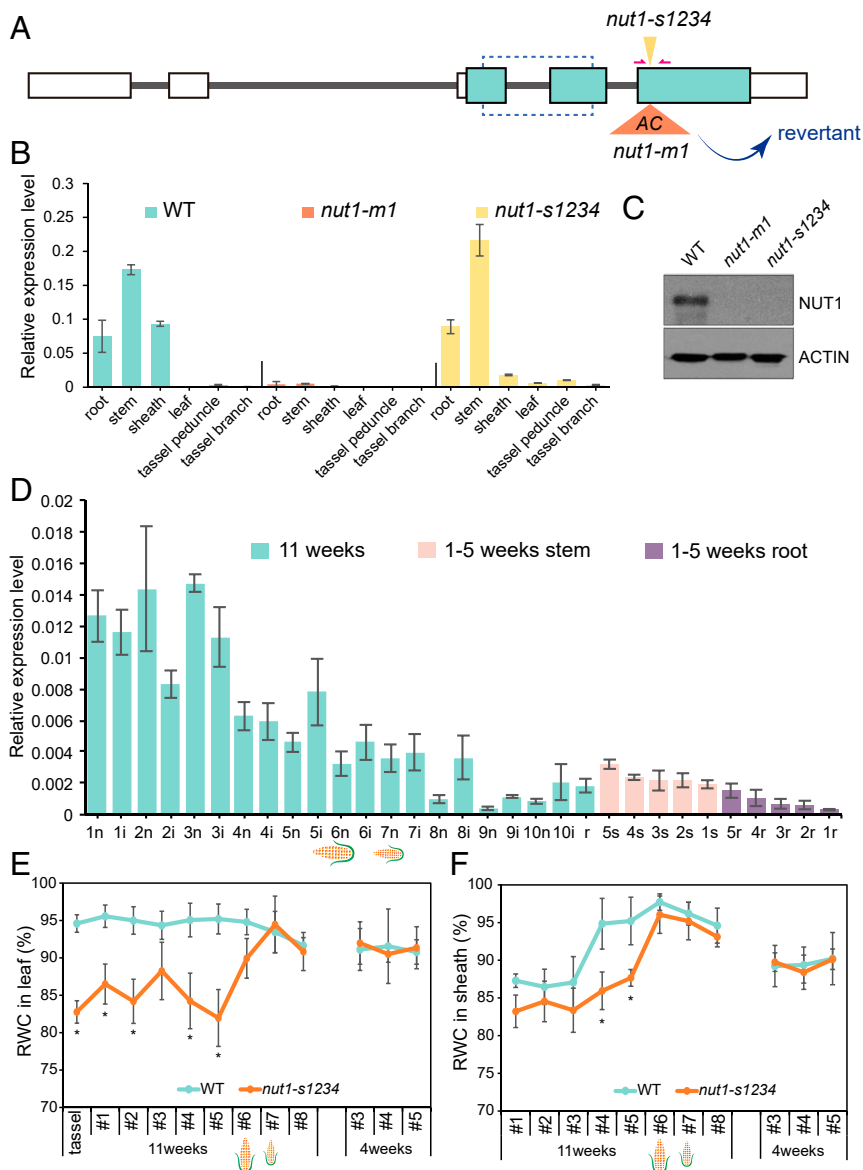

Fig. 2. Characterization of the *nut1* gene and expression. (*A*) *nut1* gene model and alleles. *nut1-m1* is caused by an *Ac* insertion into the third exon of a NAC transcription factor. The *nut1-s1234* allele has an 8-bp insertion causing a premature stop codon. A *Nut1′* wild-type revertant restoring the reading frame was isolated from *nut1-m1*, proving that the mutant phenotype is caused by the insertion. Red arrows indicate the location of primers for qRT-PCR. Blue dash lines correspond to the region of the NAC domain. Blank rectangles represent the UTRs, blue rectangles represent the exons, and lines represent introns. (*B*) Tissue specificity of *nut1* expression as indicated by qRT-PCR of 6-wk-old plants. (*C*) Western blot using a NUT1 antibody showing protein accumulation in wild-type stems, but not in either allele. *Bottom* is ACTIN loading control. (*D*) Quantification of *nut1* expression by qRT-PCR of 1- to 5-wk-old roots (mixed samples containing primary, seminal, and crown roots; purple bars), dissected shoot apices (pink bars), and aerial nodes (n) and internodes (i) from entire 11-wk flowering plants (turquoise bars) starting from the base (node 10) to the uppermost node below the tassel (node 1). Nodes 6n and 7n normally produce ears in this genetic background, and floral induction normally occurs in node 8. R, root. (*E* and *F*) RWC measurement in leaves (*E*) and sheaths (*F*) of 11-wk-old and 4-wk-old wild type (turquoise lines) and mutant (orange lines). Numbers on *x* axis refer to leaf number counting from tassel #1 (*E*) or apex (*F*) going toward the ground. The asterisks indicate statistical significance by *t* test at $P < 0.05$. The error bars in *B*, *D*, and *F* are SD from three replicates in *B* and *D* and five replicates in *E* and *F*.

Dong et al.

www.manaraa.com

defect, dye movement assays were performed. As expected, floral nodes of *nut1* mutants have difficulty moving water compared to wild type based on the lack of dye movement in both leaf sheath (Fig. 1*C*) and the uppermost stem internodes (Fig. 1*D* and Movie S1), confirming that *nut1* promotes water transport specifically to the growing floral apex. Secondary growth characteristics associated with drought and water stress are also seen in *nut1*, including reduced plant height (*SI Appendix*, Fig. S2) and reduced ear length (Fig. 1*E*).

nut1 Encodes a Protoxylem-Specific *NAC* Gene Expressed Postflowering.

To understand the molecular function of *nut1*, the gene (*GRMZM2G041668*) was cloned by isolating the sequence flanking *Ac* in the *nut1-m1* allele. The *nut1-m1* allele has an *Ac* element inserted in the third exon (Fig. 2*A*), while the *nut1-s1234* allele has an 8-bp insertion footprint produced by *Ac* excision that results in a frameshift and premature stop codon (Fig. 2*A*). Since *Ac* excision can also restore gene function at a low frequency, we conducted a genetic screen for reversion of *nut1-m1*, and identified one *Nut1′* revertant allele with a restored wild-type phenotype (*SI Appendix*, Fig. S3). Not surprisingly from an *Ac* insertion in an exon, the *Nut1′* revertant was a +0 event (28), i.e., it restored the original sequence without leaving a footprint (Fig. 2*A*). These results confirm that the mutated *GRMZM2G041668* gene is the cause of the *nut1* phenotype.

nut1 encodes NAC91, a member of the NAC transcription factor family. Within this large family, NUT1/NAC91 groups with the secondary cell wall *NAC* genes (*SWNs*) group that serve as master regulators of secondary cell wall biosynthesis (*SI Appendix*, Fig. S4) (29). Within the *SWNs*, seven members identify as *VASCULAR-RELATED NAC-DOMAIN* (*VND*) genes in *Arabidopsis* and can induce transdifferentiation of cultured cells into xylem vessel elements (19, 30). Compared to *nut1*, these *VND* orthologs have similar expression patterns and are highly redundant during xylem vessel development, displaying no obvious phenotype in any single mutant (19, 30). The *nut1* gene clusters in the same subclade as *VND4*, *5*, and *6*, implying that it may also function as a transcription regulator during xylem vessel formation. It is intriguing to note that despite the ancient genome-wide duplication in maize, the duplicate of *nut1* appears to have been lost and forms a relatively independent subclade compared to *VND4*, *5*, and *6* in *Arabidopsis*. This fact explains why the *nut1* single mutant displays a strong phenotype compared to its functionally redundant paralogs in *Arabidopsis*.

Analysis of the *nut1* expression pattern by qRT-PCR showed that *nut1* transcripts accumulate in several vascularized tissues, including root, stem, and sheath, but not leaf blade or tassel where the phenotype is found. This suggests that the necrotic phenotype itself is not a direct effect of the mutation, but a consequence of the water deficits elsewhere in the plant (Fig. 2*B*). No *nut1* expression could be detected in *nut1-m1*, confirming that it is a null allele (Fig. 2*B*). Interestingly, *nut1* expression levels in the *nut1-s1234* allele are comparable to wild type, suggesting that the frameshift mutation does not affect transcript stability (Fig. 2*B*). An antibody against the C terminus outside of the NAC domain was raised and purified. The specificity of the antibody was confirmed by Western blot, as a specific band could be detected only in wild-type stem tissue, but not in either mutant allele (Fig. 2*C*). This result demonstrates that *nut1-s1234* is a null allele since it produces no functional protein despite having normal transcript levels.

nut1 shoot and root tissue was sampled every week for 5 wk, and expression significantly increased after 4 wk (Fig. 2*D*), indicating that *nut1* may be florally induced. Other stress treatments such as drought, however, do not induce *nut1*. A survey of 96 maize RNA sequencing (RNA-seq) datasets drawn from 24 drought experiments performed on several mature and juvenile tissues showed that *nut1* was not differentially expressed (31). A survey of *nut1* expression in all of the above ground plant organs pre- and postflowering confirmed that it is temporally regulated since transcripts are barely detectable in juvenile tissues (Fig. 2*D*), progressively increases in stems and internodes of 11-wk-old flowering plants, and is highly expressed in the uppermost flag leaves. Furthermore, the sheath and stem nodes above the ear showed higher levels of *nut1* expression than those below the ear, consistent with the *nut1* necrotic phenotype being restricted to floral nodes. To correlate this temporal and tissue-specific expression with the ability to move water, relative water content (RWC) was sampled in both blade and sheath of florally induced versus juvenile leaves. *nut1* florally induced leaves showed significant reduction in RWC, whereas no change was seen in tissues below the ear, or in any juvenile samples (Fig. 2 *E* and *F*) compared to wild type. Taken together, these results show that *nut1* promotes water movement to distal apical tissues, especially after flowering.

To further understand the association between *nut1* expression and vascular development, we investigated NUT1 protein accumulation using immunolocalization. NUT1 expression is found in differentiating vascular bundles (Fig. 3*A*), but not in those of the mutant (Fig. 3 *A*, *Inset*). NUT1 consistently accumulates in the nuclei of single tracheid cell precursors that will differentiate into protoxylem in provascular strands (Fig. 3 *C* and *D*). This protoxylem-specific accumulation pattern is consistent in stem (Fig. 3*A*), sheath (Fig. 3*B*), and root vascular tissues (Fig. 3 *E* and *F*), and correlates with the developmental time course of protoxylem ontogeny within vascular bundles (Fig. 3 *G* and *H*). For example, NUT1 is found in nuclei of very early differentiating protoxylem cells (Fig. 3*I*), disappears after those protoxylem mature and secondary cell walls are made (Fig. 3*J*), and then reappears in adjacent cells that form a new protoxylem in an ordered series (Fig. 3 *J–L*), until the metaxylem initiates (Fig. 3 *K* and *L*). Interestingly, no NUT1 signals were detected in metaxylem nuclei (Fig. 3 *K* and *L*), despite the fact that metaxylem cells display defects in dye movement (Fig. 1*D*), suggesting a noncell autonomous effect of *nut1* protoxylem development on metaxylem function.

Genome-Wide Identification of the Direct Downstream Targets of NUT1.

While SWNs have been demonstrated to be master regulators of cell wall biosynthesis in dicots, there is no understanding of their direct targets in monocots (22, 32, 33). To address this problem, we performed DNA affinity purification sequencing (DAP-seq) to identify genome-wide binding events of NUT1 (34). In total, 5,127 peaks bound by NUT1 were identified (Dataset S1). An analysis of their genomic distribution showed that the majority of these peaks (78.3%) were enriched in genic regions, with only 21.7% mapping to intergenic regions (Fig. 4*A*). Within the genic peaks, NUT1 shows the highest preference for binding to proximal promoter regions located up to 1 kb upstream of the TSS (transcription start site) (Fig. 4 *A* and *B*). NUT1 also showed preferential binding to distal downstream regions and introns that comprise 20.7% and 17.2% of all peaks, respectively (Fig. 4*A*). We correlated the peaks with putative target genes by requiring the peaks to map within 10 kb upstream to 5 kb downstream of the gene. After applying this filter, 3,817 genes were identified as potential NUT1 direct targets (Dataset S2).

Transcription factors typically bind to a broad range of similar sequences that can be represented as binding motifs. The analysis of the sequences underlying the NUT1 binding peaks revealed a TTGCTT motif as the most enriched core sequence, and a 17-nt motif consisting of two partial reverse complements similar to the above sequence as the second most enriched motif. Both motifs were positioned predominantly at the summit of the peaks (Fig. 4 *C* and *D*). Interestingly, both the core motif and the 17-nt motif differed from the binding motif previously found in *Arabidopsis* VNDs (35). This divergence in DNA binding affinity
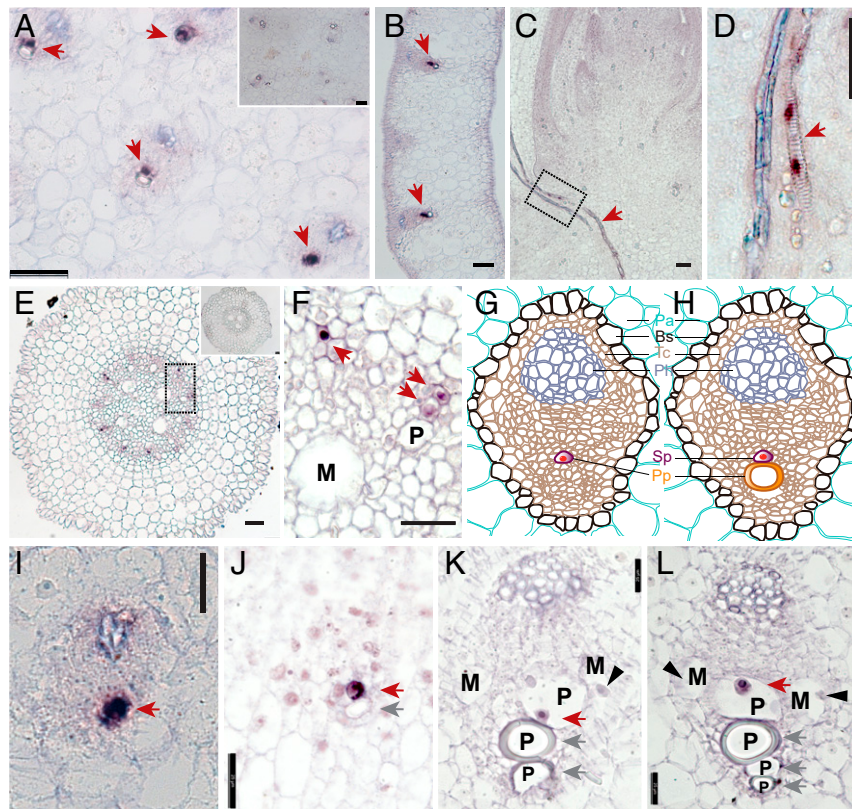
PLANT BIOLOGY

www.manaraa.com

Fig. 3. NUT1 accumulates in protoxylem precursor cells. (*A*) NUT1 immunolocalization of transverse sections of wild-type stem (*A*) and sheath (*B*) showing protein accumulation in early initiating protoxylem cells (red arrow). Control probing of *nut1-m1* mutant is *Inset* in *A* and shows no expression. All tissues were from 6-wk-old florally induced plants. (*C*) NUT1 immunolocalization on longitudinal sections of shoot apex. (*D*) Magnification of the region framed by box in *C*, showing nuclear localization in protoxylem provascular strand (red arrow). (*E*) NUT1 immunolocalization on transverse sections of primary root tip. *nut1* mutant root is *Inset*. (*F*) Magnification of the region framed by box in *E*, showing nuclear localization in root protoxylem (red arrows) differentiating in a series outwards from metaxylem. (*G* and *H*) Schematic of progression of protoxylem initiation during sheath development. After the initial protoxylem undergoes cell death the adjacent distal cell differentiates into the next one. Pa, parenchyma; Bs, bundle sheath; Tc, tracheid cells; Ph, phloem; Pp, primary protoxylem; Sp, secondary protoxylem. (*I*) Sheath vascular bundle showing NUT1 accumulation in future protoxylem (red arrows). (*J* and *K*) After the primary protoxylem cell undergoes cell death and has formed a secondary cell wall (gray arrows), the adjacent NUT1-expressing cell becomes the next protoxylem. (*K* and *L*). At later stages, NUT1 was not detected in initiating metaxylem cells (black arrowheads). (Scale bar, 50 μm in *A*–*F* and 25 μm in *I*–*L*.) P, protoxylem; M, metaxylem.

may suggest a distinct downstream regulatory network between maize and *Arabidopsis* (32, 35, 36).

To further substantiate the putative NUT1 downstream network, we performed RNA-seq using the apical stems and sheaths from 8-wk-old plants, at which stage *nut1* transcripts are present at high levels, but before associated water deficit phenotypes manifest. Compared to wild type, 2,960 differentially expressed genes (DEGs) were found in the *nut1* mutant (Fig. 4*E*), consisting of approximately equal numbers of down- and up-regulated genes (Fig. 4*F* and Dataset S3). Of the putative DAP-seq target genes, 332 were differentially expressed in *nut1* (Fig. 4*E*). These corresponded to 140 down-regulated genes and 192 up-regulated genes (Fig. 4*F*). This indicates that NUT1 could function as both a transcriptional activator and repressor, possibly depending on the presence of interacting cotranscription factors. This situation seems likely, given that VND7 in *Arabidopsis* can be either a transcriptional activator or a repressor depending on its interaction with other cofactors such as VNI2 (20, 22, 37).

Functional gene ontology (GO) analysis revealed that the largest fraction of putatively targeted down-regulated DEGs were in the cell wall macromolecule metabolism category (38) (Fig. 4*G*). The down-regulated DEGs are also enriched for genes within transcription factor pathways and signaling responses

(Fig. 4*G*), while the up-regulated DEGs are enriched in pathways involved in hormone response, particularly auxin and jasmonic acid (Fig. 4*H*). These results suggest that NUT1 may control a broad range of biological processes to promote increased water transport. One potential mechanism, consistent with the *nut1* phenotype, is through controlling secondary cell wall biosynthesis to allow cells to withstand the high negative pressures required to move water under tension. With respect to this GO term, NUT1 functions mainly as a transcriptional activator since most of these putative target genes are down-regulated in the mutant.

NUT1 Directly Controls Cellulose Biosynthesis and Apoptosis during Protoxylem Development. Several genes involved in cellulose biosynthesis and apoptosis were differentially expressed (mostly down-regulated) in the *nut1* mutant (Fig. 5 *A*–*C*). Several of these genes were also bound by NUT1 via DAP-seq and validated using the NUT1-specific antibody for chromatin immunoprecipitation (ChIP)-qPCR (Fig. 5 *D* and *E*). For example, GRMZM2G142898, annotated as *cellulose synthase 12* (*cesa12*) in maize, is the close ortholog of *Arabidopsis CELLULOSE SYNTHASE 7/IRREGULAR XYLEM 3* (*CESA7/IRX3*), which functions in secondary cell wall biosynthesis in xylem (40, 41). By ChIP-qPCR, NUT1 directly binds to the 3′ proximal end of
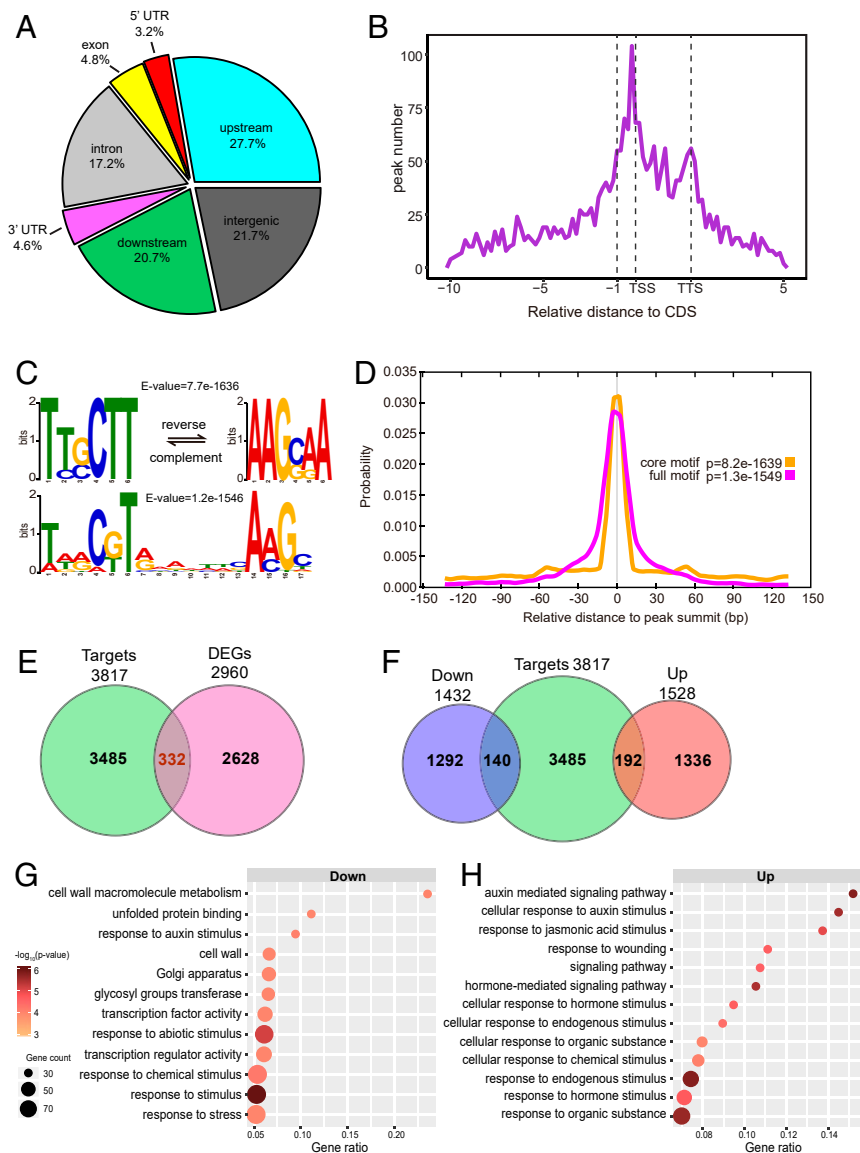
Dong et al.

www.manaraa.com

Fig. 4. Genome-wide overview of the regulatory network downstream of *nut1*. (*A*) Genome-wide distribution of NUT1 binding peaks revealed by DAP-seq. (*B*) Distribution of NUT1 binding peaks relative to gene models, showing strong enrichment within 1 kb upstream of TSSs. (*C*) Enriched motifs within the NUT1 binding peaks. The TTGCTT motif shows up as the most enriched core sequence, and the second most enriched is a 17-nt motif consisting of two partially reverse complements with high similarity to the core sequence. E-value was calculated by MEME. (*D*) Localization of the motifs relative to the NUT1 peak summits. (*E*) Overlap of all NUT1 target genes and DEGs in the *nut1* mutant. $P < 0.0001$ by hypergeometric test. *F* is the same as *E* with up- and down-regulated DEGs separated. (*G* and *H*) Functional categories of down- (*G*) and up-regulated (*H*) DEGs using agriGO v2 (39). Greater than 23% of all cell wall metabolism genes are DEGs. Bubble size indicates the number of differentially expressed gene counts in the corresponding GO category, and *x* axis indicates the relative ratio to all genes within that GO category.

cesa12, and its expression was also reduced in *nut1* mutant (Fig. 5 *A* and *B*). Similarly, other maize cellulose synthases such as *cesa6* and *cesa-like C12* were also found to be directly bound and modulated by NUT1. In addition, the *Arabidopsis* gene *COBRA* encodes a glycosylphosphatidylinositol-anchored protein that facilitates cellulose crystallization and microfibril orientation in the cell wall (42, 43). One of the maize *COBRA* orthologs, GRMZM2G071970, is bound by NUT1 (Fig. 5*A*) and also down-regulated in the mutant. Programmed cell death (PCD) in the xylem occurs soon after secondary cell wall biosynthesis to allow the cells to serve as empty vessels for long-distance transport (44). One such PCD gene is a *XYLEM CYSTEINE PEPTIDASE 1* (*XCP1*) that functions in autolysis during the differentiation of xylem tracheary elements (45, 46).

GRMZM2G066326 is the maize ortholog of *XCP1*, and is a direct NUT1 target, as are similar genes targeted by VND7 in *Arabidopsis* (22).

To further validate the finding that NUT1 targets secondary cell wall genes, we examined secondary cell wall biosynthesis and apoptosis in *nut1* protoxylem. An examination of protoxylem cells by cryofracture scanning electron microscopy (SEM) revealed thinner secondary cell wall thickness of mature protoxylem vessels in both *nut1* alleles compared to wild type (Fig. 6 *A* and *B*), consistent with observations seen in plastic sections (*SI Appendix*, Fig. S5). Given that NUT1 directly controls cellulose synthases, we examined whether cellulose defects could be observed in *nut1* mutants. We used a cellulose-specific stain, Direct Red 23 (47), to compare the cellulose content of wild type to
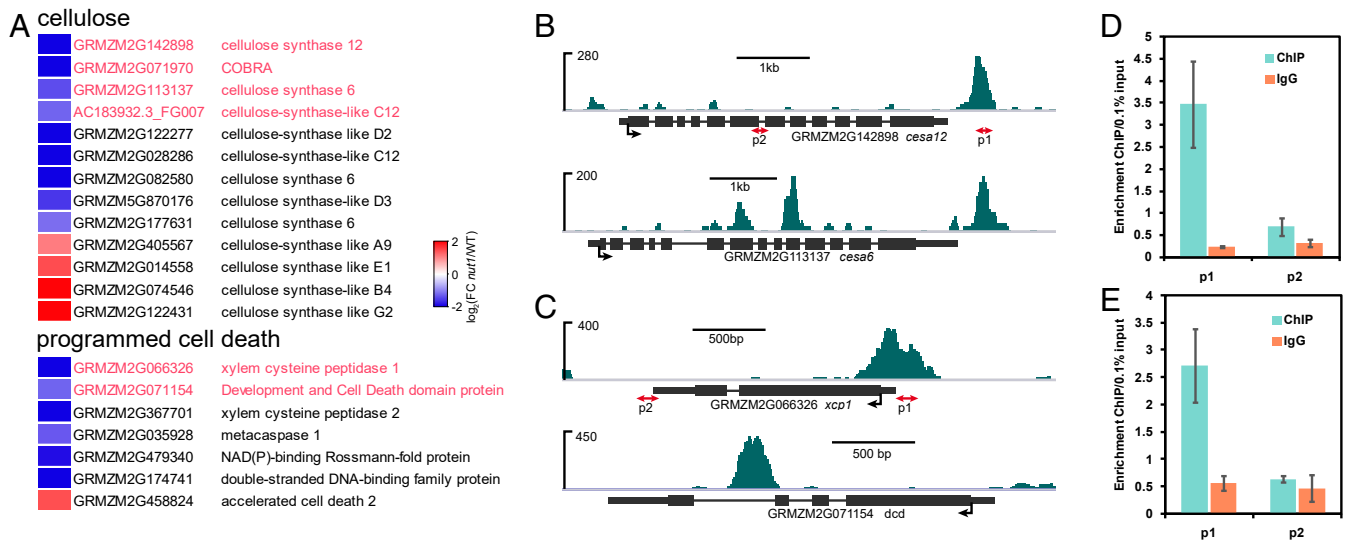
PLANT BIOLOGY

www.manaraa.com

Fig. 5. NUT1 targets genes involved in cellulose biosynthesis and apoptosis. (*A*) Heat maps showing that genes involved in cellulose biosynthesis and programmed cell death were differentially expressed in *nut1*. Gene names highlighted in red were also bound by NUT1 via DAP-seq. The gradient color scale indicates the $\log_2$ value of expression fold change (blue is down- and red is up-regulated). (*B*) NUT1 binds preferentially to the 3′ end of the top two cellulose synthase genes (*cesa12* and *cesa6*) that also show reduced expression in *nut1*. (*C*) NUT1 binds to the 5′ end and third intron, respectively, of the top two programmed cell death genes (*xcp1* and *dcd*) that show reduced expression in the mutant. (*D* and *E*) ChIP qPCR validating NUT1 binding to the genic regions of *cesa12* (*D*) and *xcp1* (*E*). ChIP was conducted using NUT1 antibody, and IgG was used as negative control. The positions of the p1 and p2 primers used for ChIP-qPCR are indicated by red arrows in *B* and *C*. The error bars represent SD from three biological replicates.

nut1. Cellulose in *nut1* was specifically reduced in the secondary cell wall of the protoxylem, whereas cellulose in the metaxylem and phloem appeared unaffected (Fig. 6 *C* and *D*). Xylans are known to comprise a major structural component of xylem secondary cell walls (48). Immunolocalization of secondary cell wall xylans was performed using a specific antibody LM10 (49) that marks protoxylem and also found to be reduced in *nut1* (Fig. 6 *E* and *F*). Intriguingly, the protoxylem annular thickenings are not only thinner in *nut1*, but also are decreased in number (Fig. 6 *G* and *H*). Together, these results suggest that the defects in the synthesis of cell wall components in *nut1* result in abnormal protoxylem secondary cell wall thickening and annular ring number. This decrease in annular ring number in the mutant is consistent with the decrease in ring number we observe in non-*nut1*-expressing tissue such as juvenile sheath protoxylem, compared to adult flag sheath protoxylem that expresses *nut1* at high levels (*SI Appendix*, Fig. S6).

These *nut1* protoxylem phenotypes, however, may not fully explain the lack of water movement in the entire vascular bundle, since the metaxylem should theoretically still be capable of transport. Using transmission electron microscopy (TEM) to examine metaxylem cell walls, we found thinner secondary cell walls with uneven surfaces in early *nut1* metaxylem (*SI Appendix*, Fig. S7), indicating possible noncell autonomous effects from the protoxylem. To understand the physiological consequence of defective *nut1* protoxylem on fully mature metaxylem function, we dissected and cleared tissues containing vascular bundles at points blocked in dye movement (Fig. 1*C*). In these tissues we observed vessel junction points in four of seven blocked bundles in *nut1* (Fig. 6*G*). In addition, the same vascular bundles below, near, and above the dye stoppage points were sectioned and stained, and the presence of perforation plates at vessel junctions was confirmed as being near the point of dye stoppage (Fig. 6*I*). Above these points where dye failed to move, the metaxylem vessels appear partially collapsed with altered cell wall morphology. This observation suggests that the defective protoxylem cell walls in *nut1* lead to metaxylem failure and partial collapse near vessel junctions as a secondary effect. Thus, water transport

in mature florally induced vascular bundles may be tightly coupled and dependent on interactions between the metaxylem and the protoxylem.

Discussion

The initiation of sufficient numbers of vascular elements is critical for facilitating long-distance transport during growth and development. Having enough vascular elements, particularly xylem, to meet the high demand for water during flowering, and prevent drying of the tassel is fundamentally important for reproduction and yield in maize. C4 grasses in particular, require a high degree of vascularization due to Kranz anatomy (50), where each cell must be in close proximity to veins in order for photosynthesis to function efficiently. Given this necessity, it is curious that many vascular genes are temporally regulated, several being expressed only after the floral transition (16). This observation implies that vascular elements display unique characteristics during different developmental phases. Indeed, ontogenetic changes in vascular development should not be surprising given the large differences in protoxylem cell morphology observed in vascular bundles (*SI Appendix*, Fig. S6) during different developmental phases. Changes are present even within the same bundle, as seen in the first protoxylem cell that has a narrow diameter, compared to the last one that has a large diameter (Fig. 6*A*). We show that these unique vascular characteristics are organ specific, even differing in expression between compartments within organs such as sheath versus blade. Thus, vascular development is an extremely dynamic process, dependent on tissue type, location, as well as developmental phase. With regards to water movement, such unique characteristics in protoxylem are mediated by the *nut1* gene as part of a developmental program critical for reinforcing protoxylem cell walls in stems, sheaths, and roots during floral development.

***nut1* Mediates Water Transport during the Floral Stage.** Consistent with the cohesion–tension model for water movement, previous studies indicated that xylem tension in the entire maize plant
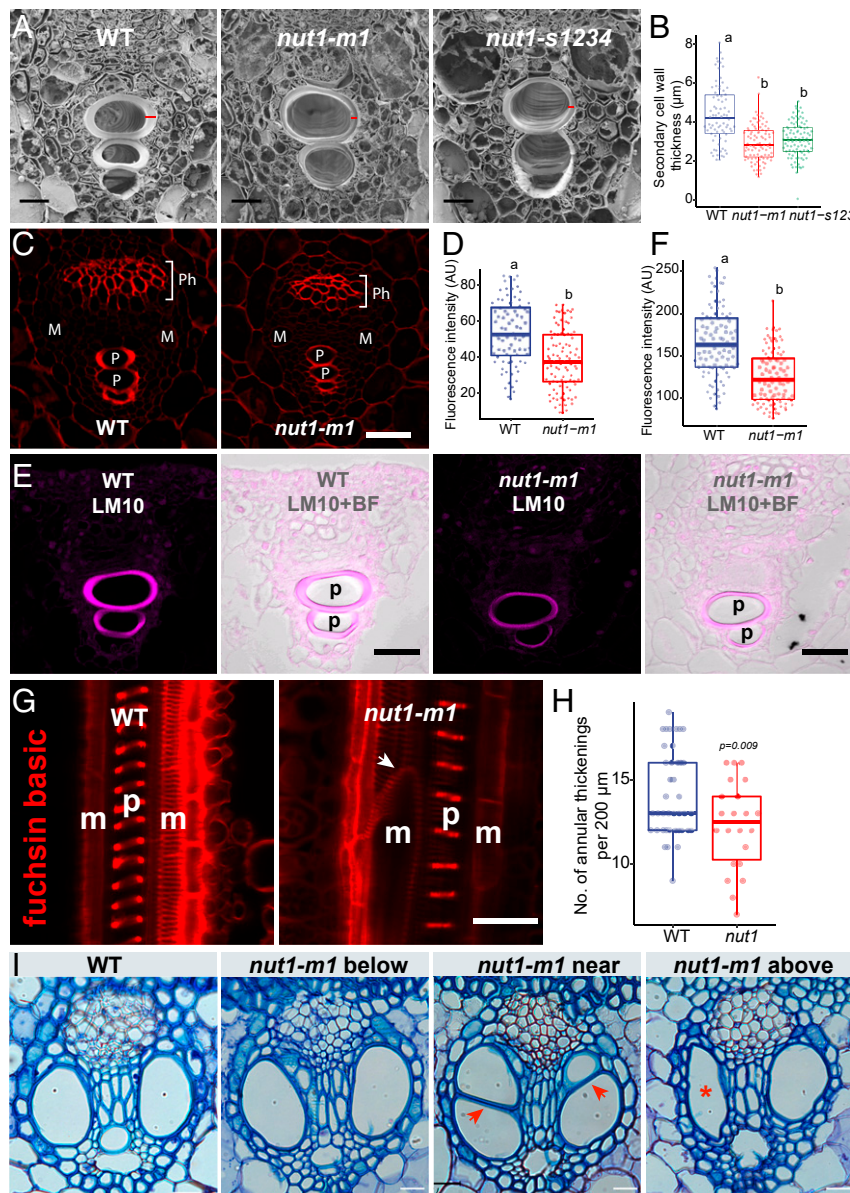
Fig. 6. Reduced *nut1* protoxylem vessel thickness caused by defective secondary cell walls. (*A*) Transverse section of a wild-type and *nut1* sheath vascular bundle by cryofracture SEM. (Scale bar, 20 μm.) (*B*) Quantitative comparison of secondary cell wall thickness of protoxylem. Red lines indicate positions where measurements were taken for each replicate. A total of 78 to 93 vascular bundles from at least seven individual plants were measured. Different letters indicate statistically significant differences at $P < 0.05$ by Tukey's test. (*C*) Confocal imaging of plastic section of vascular bundles from second apical sheath of wild-type and *nut1* flowering plants. Protoxylem cellulose was stained using Direct Red 23. (Scale bar, 50 μm.) (*D*) Quantitative comparison of the cellulose content of protoxylem as determined by normalized fluorescence intensity in *C*. For each replicate, 80 and 97 measurements were taken from four wild-type and *nut1* mutant plants, respectively. Different letters indicate statistically significant differences at $P < 0.05$ by Tukey's test. (*E*) Confocal imaging of xylan immunolocalization using the LM10 monoclonal antibody. Comparison of plastic sections of second apical sheath tissue from WT and *nut1-m1* flowering plants. Dark panels show fluorescence intensity, while light panels are the overlay with brightfield image. (Scale bar, 20 μm.) (*F*) Quantitative comparison of xylan content of wild-type and *nut1* protoxylem as determined by the normalized fluorescence intensity in *E*. For each replicate, measurements were taken on 98 individual protoxylem cells from three wild-type and *nut1* mutant plants, respectively. Statistically significant differences were detected at $P < 0.05$ by Tukey's test. (*G*) Cleared sheath tissue stained with basic fuchsin for wild type (*Left*) and *nut1* (*Right*) in areas where dye movement is blocked (as indicated by arrows in Fig. 1*C*). Lignified protoxylem (p) annular thickenings are visible in between both metaxylem vessels. Vessel junction (white arrow) was associated with blocked vessel transport. (Scale bar, 50 μm.) (*H*) Quantitative comparison of annular thickening density between wild-type and *nut1* protoxylem. All of the fluorescence images used for pairwise comparison were taken under identical microscope settings. (*I*) Transverse serial sections of W22 (*Left*) and nut1 node#1 sheath tissue subjected to dye movement assay similar to the experiment shown in Fig. 1*C*. A *nut1* vascular bundle with limited dye movement was fixed, sectioned, and stained with Toluidine Blue below, near and above the dye stoppage point, respectively. The presence of transverse cell walls (red arrows) in the metaxylem near the dye stoppage points indicate the presence of perforation plates at vessel junctions, while the metaxylem above them appear collapsed with altered cell wall morphology (red asterisk). Wild-type W22 node#1 sheath with normal dye movement was used as a control. (Scale bar, 25 μm.)

Dong et al.

www.manaraa.com

PLANT BIOLOGY

gradually increases, starting from the bottom of the plant up to the apex (11) where negative pressures are highest. Tension also increases at midday when transpiration rates and temperatures are highest, and this is likely the cause of the increased rate of cavitations during this period, especially under drought (7). In addition, maize vascular bundles fuse at each node, and the presence of perforation plates at these fusion points (51) result in increased hydraulic resistance (9), making water movement even more difficult. Because of these factors, water movement becomes progressively more difficult through each node of the plant, especially during flowering when high volumes of water are needed at the terminal and lateral apices of the plant to allow reproduction. In addition, this stage is the most vulnerable to drought stress in maize (2) in terms of yield loss. This necessitates special physiological mechanisms to accommodate the change in water requirements within the plant, something that has been indicated by recent transcriptomic studies. Indeed, several recent experiments have demonstrated that floral regulators are capable of inducing secondary xylem growth simultaneously with the floral transition in *Arabidopsis* and tomato (16, 52). On the other hand, regulatory genes, such as the floral repressor *short vegetative phase* (*svp*), dampen vascular cambium development (53), indicating that both growth and repression of vascular development are important during flowering. Overall, these results indicate that the floral transition is coordinated with accelerated vascular differentiation in multiple plants, consistent with the period when the *nut1* phenotype manifests. During this phase, dye movement assays demonstrate that *nut1* vascular bundles have difficulty transporting water in florally induced stems and sheath tissue (Fig. 1 *C* and *D*), and at points where dye movement stops there is often the presence of vessel junctions and partially collapsed metaxylem (Fig. 6 *G* and *I*). While we show that the downstream targets of *nut1* are involved in secondary cell wall biosynthesis, it is unclear if the florigen affects their expression directly, or through *nut1*. Florigen is known to be produced in phloem cells of leaves before being transported long distances to the shoot apical meristem to induce flowering (54). Because the florigen protein is known to be noncell autonomous, it is possible that it may translocate to the xylem precursors and either directly or indirectly, stimulate *nut1* gene expression. Supporting this hypothesis, CArG-box motifs that could be potentially bound by floral MADS transcription factors were found in the proximal promoter of *nut1* (*SI Appendix*, Fig. S8). Identification of potential floral factors that bind to the *nut1* promoter will be critical in unraveling the connection between *nut1* and the floral transition.

Functional Divergence of *nut1* in Monocots Compared to Dicots. *nut1* is a single-copy *NAC* transcription factor in maize with a nonredundant distinctive function, given that its duplicate was likely lost some time ago. Several *NAC* transcription factors have been identified as key regulators of xylem differentiation in *Arabidopsis*. In particular, overexpression of members of the *VND* subclade in cultured tracheary elements was found to induce xylem cell identity (55). Individual *VND* genes may have distinct roles based on gain-of-function studies, with *VND6* being responsible for the differentiation of metaxylem vessels and *VND7* functioning as a switch for protoxylem cell identity (19). This latter role for *VND7* was demonstrated by single cell transcriptomic studies using inducible constructs in which specific threshold levels were tightly associated with establishment of protoxylem cell identity (21). Loss-of-function alleles of *VND6* and *VND7* have not been reported to display any phenotypes, indicating possible functional redundancy (19). However, using dominant negative versions of *VND6* and *VND7* fused to strong repressor domains, defects in growth and root xylem vessel formation were observed (19, 56). Using immunolocalization, we discovered that NUT1 accumulates in single cells initiating as

protoxylem vessels (Fig. 3 *I* and *J*), but is absent from differentiating metaxylem (Fig. 3 *K* and *L*). This observation suggests that *nut1* may function to help pattern protoxylem vessels much like *VND7*, despite the fact that it is phylogenetically closer to *VND6* (*SI Appendix*, Fig. S4). The floral specific phenotypes of *nut1* have not been reported for other *VND* mutants of *Arabidopsis*, and this may imply additional species-specific functional divergence for NUT1 in maize. There may be several underlying reasons for such functional divergence. The vascular bundles of dicots and monocots display different developmental patterning as well as histology (57). Consistent with this, a comparison of expression profiles of highly expressed secondary cell wall-related genes in maize versus *Arabidopsis* revealed very limited orthology between the two, indicating distinct regulatory developmental networks underlying their anatomical divergence (58). Furthermore, flowering maize plants are much taller than *Arabidopsis*, making water movement considerably more difficult, especially under challenging environmental conditions. This fact may necessitate unique genetic factors such as *nut1* that facilitate cell type-specific long-distance water movement during flowering in maize.

nut1 appears to also have a unique role during protoxylem differentiation compared to other *Arabidopsis VND* genes. Its putative dicot ortholog, *VND6*, has been shown to be sufficient for protoxylem identity from gain-of-function studies, while in maize the *nut1* mutant protoxylem identity is unaffected. For example, in *nut1* mutants, the protoxylem maintains its identity based on the presence of secondary cell walls, a defining characteristic of this cell type. These secondary cell walls, however, appear to be thinner (Fig. 6*A*) and abnormal, based on direct red staining for cellulose (Fig. 6*C*) and localization of arabinoxylans (Fig. 6*E*). In addition, *nut1* secondary cell walls have fewer annular rings (Fig. 6*H*) which may lead to weakened resistance to the internal negative pressures required for long-distance water movement. Finally, transient overexpression of *nut1* in maize and barley leaf stomatal cells did not appear to confer protoxylem cell identity based on the absence of secondary cell walls or annular rings in the transformed cells (*SI Appendix*, Fig. S9). Taken together, these results indicate that *nut1* primarily functions to enhance and maintain the thickness and integrity of the secondary cell wall rather than specifying protoxylem cell identity, unlike its homologs in *Arabidopsis*. This result, however, does not preclude a role for *nut1* in specifying protoxylem identity redundantly with other *NAC* genes as has been shown in dicots (19).

A Possible Functional Relationship Between Protoxylem and Metaxylem. Interestingly, dye movement is inhibited in the *nut1* metaxylem (Fig. 1 *C* and *D*), which often displays abnormal cell walls (Fig. 6*I*), despite the fact that NUT1 is not expressed in these cells (Fig. 3 *I* and *J*). Indeed, we observed *nut1* metaxylem with thinner, irregular secondary cell wall thickenings as well as defects in the adjacent vessels (Fig. 6*I* and *SI Appendix*, Figs. S5 and S7), suggesting indirect effects of protoxylem development on metaxylem. There is increasing evidence for a more direct functional relationship between the protoxylem and metaxylem in crop plants. For example, in artificially embolized maize leaf vascular bundles (9) radial movement of water from protoxylem to metaxylem and vice versa was observed. This radial connectivity may be particularly crucial for refilling the broken water column and repairing cavitations and embolisms. In the case of *nut1*, embolisms may be present at metaxylem vessel junctions since dye movement often stopped near these points (Fig. 6 *G* and *I*). The defective *nut1* protoxylem may be incapable of helping to repair the embolism, resulting in a broken water column and metaxylem collapse in the vascular strand above (Fig. 6*I*). Metaxylem vessels are more likely to be embolized in response to heat or drought stress due to their large diameter

vessels, while the smaller diameter protoxylem vessels within the same bundle may be a more dependable water source for embolism repair. This is a critical process since up to 70% of large metaxylem vessels in the field may experience embolisms (59) and must undergo constant repair. While such embolism repair is postulated to occur at night via positive root pressure in maize (7), an alternative mode of repair via the protoxylem may offer a more immediate solution.

Functional Differences within Floral Protoxylem. The fact that *nut1* is only expressed after floral induction may be a reflection of the difficulty in moving water during this phase of development. Since maize fertilization is keenly dependent on water levels and can only occur over a 3- to 4-d window, this phase of development requires additional genetic factors such as *nut1* to support protoxylem secondary cell walls far above ground and ensure reliable water delivery. Thus, selective breeding for increased protoxylem function in specific tissues may be an effective way to combat both heat and drought stress. The fact that *nut1* only comes on after the floral transition indicates that reproductive tissues may be uniquely sensitive to such stresses. It will be useful to determine the physiological basis behind the tissue specificity of *nut1* function since the protein was only found in root, stem, and sheath, but not leaf blades or reproductive meristems that display most of the effects in the mutant. Moreover, it will be important to understand the biological basis behind the temporal specificity of *nut1* expression to the floral phase, and whether engineering for earlier expression may enhance water movement during juvenile development.

Materials and Methods

Plant Material. A previous system has been established for genetic derivation of the transposants, through a strategy of coupling of two easily scored endosperm markers, *wx* and *bz*, to monitor Ac transposition in the genetic background of maize inbred line W22 (27). The *nut1-m1* allele was selected from this system and corresponds to tac917.12 as designated in ref. 27. The *nut1* revertant screening relied on the fact that Ac has negative dosage effect. By monitoring loss of Ac activity with the *bz-m2(D1)* reporter, 20 transposed Ac alleles were isolated and phenotyped. Plants with a wild-type phenotype were selected and sequenced, and one of them was successfully validated as a wild-type revertant allele of *nut1* that restored the open reading frame (ORF). W22 was used as wild-type control for all experiments except the RNA-seq which used the *bz-m2(D1) wx* alleles. The plants were grown in the Gill Tract field in Albany, CA for the summer season or in the greenhouse of the Plant Gene Expression Center, with 25 °C 16-h light/20 °C 8-h dark regimen.

Dye Transport Assay. Tassel stems were cut from 10-wk-old plants and dipped in Coomassie blue dye for 4 h. Transverse hand sections with ∼0.5-mm thickness were taken at the same distance (1 cm) from the dye level. Microscope images were taken under a stereomicroscope (Leica, MZ16F).

RWC. Whole tassels, 5-cm segments of leaf blades or 2-cm segments of sheath tissue, respectively, were harvested and placed into sealed Ziploc bags to avoid weight loss by evaporation. The sealed samples were weighed by a milligram analytical balance, and the tissue fresh weight (FW) was calculated by subtraction of the bag weight. A total of 20 mL of water was added into each plastic bag, ensuring that all of the tissue was submerged, and placed in the dark at room temperature for 36 h. The tissues were then removed from the bags and paper towels were used to gently absorb excess water on the tissue surface. The tissue was weighed to obtain a turgid weight (TW) value. The tissue was transferred into an oven at 60 °C for 4 d, and the dry weight (DW) was measured. The relative water content was calculated as RWC (%) = [(FW − DW)/(TW − DW)] × 100.

Phylogenetic Analysis. Protein sequences for NUT1 orthologs were obtained by BLAST searching in TAIR (https://www.arabidopsis.org/) and EnsemblPlants (http://plants.ensembl.org/index.html). Multiple sequence alignments were performed using CLUSTALW, and following phylogenetic analyses were conducted through MEGAX using the maximum likelihood method (60).

Gene Expression Quantification by RT-qPCR. Total RNA was isolated from various tissue samples harvested using TRIzol Reagent (Invitrogen, Cat. No. 15596026) according to manufacturer's instructions. For qRT-PCR analysis, cDNA was synthesized from DNase I-treated total RNA as described previously (61). SD was calculated among three biological replicates for each sample. *ZmGAPDH* was used as the internal reference to normalize the expression data. The primers used for qPCR are listed in Dataset S4.

Antibody Generation and Immunolocalization. Full-length NUT1 coding sequence was cloned into the pET21d expression vectors (Novagen), and the antigen was purified and injected into guinea pigs. The serum was affinity purified using the recombinant NUT1 protein, as described by ref. 62 using standard protocols approved by the Association for Assessment and Accreditation of Laboratory Animal Care (AAALAC 000868). Anti-guinea pig alkaline phosphatase secondary antibody (Thermo Fisher, A18772) was used as the secondary antibody.

For the immunolocalization of xylan, LM10 monoclonal antibody was used as the primary antibody in a 1:100 dilution. A goat anti-rat monoclonal antibody conjugated with Alexa Fluor 488 was used as a secondary antibody. Respective immunolocalization of NUT1 and LM10 were performed as previously described (63). The immunolocalization signal of NUT1 was visualized using a compound microscope under brightfield, and the LM10 immunolocalization was visualized with 488-nm excitation and image detected at 515 to 530 nm in a Leica TCS SP8 confocal microscope.

DAP-Seq and Data Analysis. Library preparation: Illumina genomic DNA library was prepared according to Bartlett et al. (64). In brief, 5,000 ng of maize B73 phenol:chloroform purified genomic DNA from developing maize ears was diluted in elution buffer (EB) (10 mM Tris·HCl, pH 8.5) sheared to 200-bp fragments using a Covaris S2 and size selected using prepared SeraMag beads at a ratio of 2:1 beads to DNA. Eluted DNA was end repaired using the End-It kit (Lucigen) according to the manufacturer's recommendations. End-repaired DNA was purified using the Qiagen QIAquick PCR purification protocol and subsequently A tailed using Klenow 3′-5′ exo- (NEB). A-tailed DNA was purified using the Qiagen QIAquick PCR purification protocol. Purified DNA was ligated to truncated Illumina adapters overnight at 16 °C using T4 DNA ligase (NEB). The adapter-ligated library was purified using Ampure XP size selection beads at a 1:1 beads to DNA ratio.

Clone preparation and protein expression was as follows: The full-length NUT1 coding sequence was recombined into the pIX-HALO vector (64) using LR Clonase II (Life Technologies). HALO-NUT1 protein was subsequently generated using 1,000 ng of pIX-HALO-NUT1 plasmid and the TNT rabbit reticulocyte in vitro expression system (Promega) according to the manufacturer's recommendations. The reaction was then immediately incubated with 10 μL of Magne-HALOTag beads (Promega) for 1 h at room temperature in 1× PBS with 0.005% Nonidet P-40 (PBST). Bound protein was washed six times with PBST and subsequently incubated with 1,000 ng of adapter-ligated genomic DNA library for 1 h at room temperature. Beads were washed eight times with PBST and eluted with EB by heating samples at 98 °C for 10 min. The eluted DNA was transferred to a new tube and PCR enriched as described in ref. 64 prior to sequencing on an Illumina NextSeq 500 using 75-bp single-end reads.

DAP-seq reads were trimmed and mapped to the maize B73v3 genome as described in ref. 32. Reads mapping to more than one location were filtered to retain only those with >MAPQ30 using samtools (samtools view -b -q 30). Peak calling was performed using the GEM peak caller (v2.5; ref. 65) as described in ref. 34. Bigwig files were used to visualize the peaks in the integrative genomics viewer (66). Motif calling was performed using meme-chip with default parameters (67) and input sequences comprising 150 bp upstream and downstream of the peak summit.

ChIP-qPCR. From 8-wk-old plants, apical stems and sheath (∼5 mm) with decapitated tassel primordia were harvested and fixed in 1% formaldehyde for 15 min. The ChIP experiment was performed following previously described protocols (63). Three biological replicates of immunoprecipitated DNA in ChIP were applied for each qPCR reaction using the primer pairs listed in Dataset S4. Enrichment levels were normalized to 0.1% of input, and IgG served as a negative control.

RNA-Seq and Data Analysis. The same tissues used for RNA-seq were also used for ChIP-qPCR. Samples from seven siblings were pooled as one biological repeat; three biological repeats were performed for wild type and *nut1-s1234*. Total RNA was extracted with TRIzol reagent (Invitrogen, Cat. No. 15596026). Library construction was performed using ScriptSeq v2 RNA-Seq Library Kit (Epicenter, Cat. No. SSV21106) according to manufacturer's

Dong et al.

www.manaraa.com

instructions and then sequenced on a HiSeq 2500 sequencer for 150 single-end reads. All of the clean reads were trimmed by Trimmomatic v.0.36 and mapped to the maize B73 v3 genome using STAR aligner v.2.6.0a with default parameter settings (68). Counted reads were tested for differential expression with edgeR using false discovery rate (FDR) significance threshold of 0.05 (69, 70). Gene ontology analysis was performed through agriGO v2.0 (39), and the results were visualized using ggplot2 in R.

Microscope Imaging. For the transmission electron microscopy, tissue was dissected in about ∼3- to 4-mm squares; fixed overnight in 2.0% formaldehyde, 2.5% glutaraldehyde, 2.5 mM CaCl₂, and 0.1 M sodium cacodylate buffer (pH 6.9); rinsed in 0.1 M sodium cacodylate buffer (pH 6.9) three times for 20 min each; postfixed in 1% aqueous osmium tetroxide for 2 h; and then rinsed in water three times for 20 min. Then the tissue was dehydrated in a graded acetone series 20 min per step: 30%, 50%, 70%, 85%, and 95% and lastly dehydrated in 100% acetone three times for 30 min. The tissue was subsequently infiltrated with resin in a graded series of acetone:resin mixture (33% resin in acetone, 50% resin in acetone, 66% resin in acetone, 100% resin) for 1 h for each step, exchanged for fresh resin, and the tissue infiltrated at a rotator overnight and then embedded into molds in a 60 °C oven. Ultrathin sections were cut on an ultramicrotome and imaged with a JOEL 1200 transmission electron microscope.

For the cryofracture scanning electron microscope, samples were dehydrated in a graded series of ethanol (30%, 50%, 70%, 95%, and 3 × 100%, 30 min per exchange) and cryofractured in liquid nitrogen. Cryofracturing consists of dropping the dehydrated tissue into liquid nitrogen and fracturing

with a prechilled razor blade held in a vice grip. The tissue pieces were collected with chilled tweezers, returned to 100% ethanol, and critical point dried in a Tousimis Autosamdri-815 critical point dryer. The tissue pieces were then mounted onto aluminum specimen stubs using double adhesive coated carbon tabs (Ted Pella, Inc.), and the mounted samples coated with gold palladium in a Denton Desk II (Denton Vacuum, Inc.) sputter-coating unit. The samples were viewed and photographed in a JEOL JSM-7900F field emission scanning electron microscope.

For the cellulose staining, 0.1% Direct Red 23 solution was prepared and plastic sections were stained for 10 min and washed in PBS for 30 min with gentle shaking. The stained sections were viewed with 561-nm excitation and images detected at 580 to 615 nm in a Leica TCS SP8 confocal microscope. All of the replicate images were taken under a consistent setting of the microscope. The measurement of fluorescence intensity was performed using ImageJ 2.0.0 on the original images by selecting 1 × 1 μm square selections in the center of the secondary cell wall for each protoxylem, and subtracting a value within the same sized selection from the background.

1. Food and Agriculture Organization of the United Nations, Water supply and crop yield. http://www.fao.org/land-water/databases-and-software/crop-information/maize/en/. Accessed 13 March 2020.
2. K. Begcy et al., Male sterility in maize after transient heat stress during the tetrad stage of pollen development. Plant Physiol. 181, 683–700 (2019).
3. H. A. Hussain et al., Interactive effects of drought and heat stresses on morpho-physiological attributes, yield, nutrient uptake and oxidative status in maize hybrids. Sci. Rep. 9, 3890 (2019).
4. P. A. Henckel, Physiology of plants under drought. Annu. Rev. Plant Physiol. 15, 363–386 (1964).
5. C. Lesk, P. Rowhani, N. Ramankutty, Influence of extreme weather disasters on global crop production. Nature 529, 84–87 (2016).
6. M. T. Tyree, J. S. Sperry, Vulnerability of xylem to cavitation and embolism. Annu. Rev. Plant Physiol. Plant Mol. Biol. 40, 19–36 (1989).
7. M. T. Tyree, E. L. Fiscus, S. D. Wullschleger, M. A. Dixon, Detection of xylem cavitation in corn under field conditions. Plant Physiol. 82, 597–599 (1986).
8. M. Canny, Embolisms and refilling in the maize leaf lamina, and the role of the protoxylem lacuna. Am. J. Bot. 88, 47–51 (2001).
9. B. G. Hwang, J. Ryu, S. J. Lee, Vulnerability of protoxylem and metaxylem vessels to embolisms and radial refilling in a vascular bundle of maize leaves. Front. Plant Sci. 7, 941 (2016).
10. P. Ramachandran, G. Wang, F. Augstein, J. de Vries, A. Carlsbecker, Continuous root xylem formation and vascular acclimation to water deficit involves endodermal ABA signalling via miR165. Development 145, dev159202 (2018).
11. C. Wei, M. T. Tyree, E. Steudle, Direct measurement of xylem pressure in leaves of intact maize plants. A test of the cohesion-tension theory taking hydraulic architecture into consideration. Plant Physiol. 121, 1191–1206 (1999).
12. G. S. Chuck et al., Overexpression of the maize Corngrass1 microRNA prevents flowering, improves digestibility, and increases starch content of switchgrass. Proc. Natl. Acad. Sci. U.S.A. 108, 17550–17555 (2011).
13. J. A. Orkwiszewski, R. S. Poethig, Phase identity of the maize leaf is determined after leaf initiation. Proc. Natl. Acad. Sci. U.S.A. 97, 10631–10636 (2000).
14. I. M. Morrison, Changes in the lignin and hemicellulose concentrations of ten varieties of temperate grasses with increasing maturity. Grass Forage Sci. 35, 287–293 (1980).
15. V. I. Cheadle, Specialization of vessels within the xylem of each organ in the Monocotyledoneae. Am. J. Bot. 31, 81–92 (1944).
16. A. Shalit-Kaneh et al., The flowering hormone florigen accelerates secondary cell wall biogenesis to harmonize vascular maturation with reproductive development. Proc. Natl. Acad. Sci. U.S.A. 116, 16127–16136 (2019).
17. H. Shao, H. Wang, X. Tang, NAC transcription factors in plant multiple abiotic stress responses: Progress and prospects. Front. Plant Sci. 6, 902 (2015).
18. T. Demura et al., Visualization by comprehensive microarray analysis of gene expression programs during transdifferentiation of mesophyll cells into xylem cells. Proc. Natl. Acad. Sci. U.S.A. 99, 15794–15799 (2002).
19. M. Kubo et al., Transcription switches for protoxylem and metaxylem vessel formation. Genes Dev. 19, 1855–1860 (2005).
20. M. Taylor-Teeples et al., An Arabidopsis gene regulatory network for secondary cell wall synthesis. Nature 517, 571–575 (2015).
21. G. M. Turco et al., Molecular mechanisms driving switch behavior in xylem cell differentiation. Cell Rep. 28, 342–351.e4 (2019).
22. M. Yamaguchi et al., VASCULAR-RELATED NAC-DOMAIN 7 directly regulates the expression of a broad range of genes for xylem vessel formation: Direct target genes of VND7. Plant J. 66, 579–590 (2011).

23. X. Wang et al., Genetic variation in ZmVPP1 contributes to drought tolerance in maize seedlings. Nat. Genet. 48, 1233–1241 (2016).
24. H. Mao et al., A transposable element in a NAC gene is associated with drought tolerance in maize seedlings. Nat. Commun. 6, 8326 (2015).
25. V. P. Thirumalaikumar et al., NAC transcription factor JUNGBRUNNEN1 enhances drought tolerance in tomato. Plant Biotechnol. J. 16, 354–366 (2018).
26. S. Ebrahimian-Motlagh et al., JUNGBRUNNEN1 confers drought tolerance downstream of the HD-Zip I transcription factor AtHB13. Front. Plant Sci. 8, 2118 (2017).
27. M. Cowperthwaite et al., Use of the transposon Ac as a gene-searching engine in the maize genome. Plant Cell 14, 713–726 (2002).
28. L. Scott, D. LaFoe, C. F. Weil, Adjacent sequences influence DNA repair accompanying transposon excision in maize. Genetics 142, 237–246 (1996).
29. K. Růžička, R. Ursache, J. Hejátko, Y. Helariutta, Xylem development–from the cradle to the grave. New Phytol. 207, 519–535 (2015).
30. J. Zhou, R. Zhong, Z.-H. Ye, Arabidopsis NAC domain proteins, VND1 to VND5, are transcriptional regulators of secondary wall biosynthesis in vessels. PLoS One 9, e105726 (2014).
31. Z. Miao, Z. Han, T. Zhang, S. Chen, C. Ma, A systems approach to a spatio-temporal understanding of the drought stress response in maize. Sci. Rep. 7, 6590 (2017).
32. R. Zhong, C. Lee, Z.-H. Ye, Global analysis of direct targets of secondary wall NAC master switches in Arabidopsis. Mol. Plant 3, 1087–1103 (2010).
33. K. Ohashi-Ito, Y. Oda, H. Fukuda, Arabidopsis VASCULAR-RELATED NAC-DOMAIN6 directly regulates the genes that govern programmed cell death and secondary wall formation during xylem differentiation. Plant Cell 22, 3461–3473 (2010).
34. M. Galli et al., The DNA binding landscape of the maize AUXIN RESPONSE FACTOR family. Nat. Commun. 9, 4526 (2018).
35. R. C. O'Malley et al., Cistrome and epicistrome features shape the regulatory DNA landscape. Cell 165, 1280–1292 (2016).
36. J. R. Olins et al., Secondary wall regulating NACs differentially bind at the promoter at a CELLULOSE SYNTHASE A4 Cis-eQTL. Front. Plant Sci. 9, 1895 (2018).
37. M. Yamaguchi et al., VND-INTERACTING2, a NAC domain transcription factor, negatively regulates xylem vessel formation in Arabidopsis. Plant Cell 22, 1249–1263 (2010).
38. K. Keegstra, N. Raikhel, Plant glycosyltransferases. Curr. Opin. Plant Biol. 4, 219–224 (2001).
39. T. Tian et al., agriGO v2.0: A GO analysis toolkit for the agricultural community, 2017 update. Nucleic Acids Res. 45, W122–W129 (2017).
40. N. G. Taylor, W. R. Scheible, S. Cutler, C. R. Somerville, S. R. Turner, The irregular xylem3 locus of Arabidopsis encodes a cellulose synthase required for secondary cell wall synthesis. Plant Cell 11, 769–780 (1999).
41. Y. Watanabe et al., Visualization of cellulose synthases in Arabidopsis secondary cell walls. Science 350, 198–203 (2015).
42. N. Sorek et al., The Arabidopsis COBRA protein facilitates cellulose crystallization at the plasma membrane. J. Biol. Chem. 289, 34911–34920 (2014).
43. F. Roudier et al., COBRA, an Arabidopsis extracellular glycosyl-phosphatidyl inositol-anchored protein, specifically controls highly anisotropic expansion through its involvement in cellulose microfibril orientation. Plant Cell 17, 1749–1763 (2005).
44. B. Bollhöner, J. Prestele, H. Tuominen, Xylem cell death: Emerging understanding of regulation and function. J. Exp. Bot. 63, 1081–1094 (2012).
45. U. Avci, H. Earl Petzold, I. O. Ismail, E. P. Beers, C. H. Haigler, Cysteine proteases XCP1 and XCP2 aid micro-autolysis within the intact central vacuole during xylogenesis in Arabidopsis roots. Plant J. 56, 303–315 (2008).

Dong et al.

www.manaraa.com

46. V. Funk, B. Kositsup, C. Zhao, E. P. Beers, The Arabidopsis xylem peptidase XCP1 is a tracheary element vacuolar protein that may be a papain ortholog. *Plant Physiol.* **128**, 84–94 (2002).

47. R. Ursache, T. G. Andersen, P. Marhavý, N. Geldner, A protocol for combining fluorescent proteins with histological stains for diverse cell wall components. *Plant J.* **93**, 399–412 (2018).

48. D. H. Northcote, R. Davey, J. Lay, Use of antisera to localize callose, xylan and arabinogalactan in the cell-plate, primary and secondary walls of plant cells. *Planta* **178**, 353–366 (1989).

49. L. McCartney, S. E. Marcus, J. P. Knox, Monoclonal antibodies to plant cell wall xylans and arabinoxylans. *J. Histochem. Cytochem.* **53**, 543–546 (2005).

50. O. V. Sedelnikova, T. E. Hughes, J. A. Langdale, Understanding the genetic basis of C_4 Kranz anatomy with a view to engineering C_3 crops. *Annu. Rev. Genet.* **52**, 249–270 (2018).

51. M. W. Shane, M. E. McCully, M. J. Canny, The vascular system of maize stems revisited: Implications for water transport and xylem safety. *Ann. Bot.* **86**, 245–258 (2000).

52. R. Sibout, S. Plantegenet, C. S. Hardtke, Flowering as a condition for xylem expansion in Arabidopsis hypocotyl and root. *Curr. Biol.* **18**, 458–463 (2008).

53. J. Zhang *et al.*, Transcriptional regulatory framework for vascular cambium development in Arabidopsis roots. *Nat. Plants* **5**, 1033–1042 (2019).

54. L. Corbesier *et al.*, FT protein movement contributes to long-distance signaling in floral induction of Arabidopsis. *Science* **316**, 1030–1033 (2007).

55. M. Yamaguchi *et al.*, VASCULAR-RELATED NAC-DOMAIN6 and VASCULAR-RELATED NAC-DOMAIN7 effectively induce transdifferentiation into xylem vessel elements under control of an induction system. *Plant Physiol.* **153**, 906–914 (2010).

56. K. Hiratsu, K. Matsui, T. Koyama, M. Ohme-Takagi, Dominant repression of target genes by chimeric repressors that include the EAR motif, a repression domain, in Arabidopsis. *Plant J.* **34**, 733–739 (2003).

57. P. H. Raven, R. F. Evert, S. E. Eichhorn, *Biology of Plants*, (Macmillan, 2005).

58. B. W. Penning *et al.*, Expression profiles of cell-wall related genes vary broadly between two common maize inbreds during stem development. *BMC Genom.* **20**, 785 (2019).

59. M. E. McCully, Root xylem embolisms and refilling. Relation to water potentials of soil, roots, and leaves, and osmotic potentials of root xylem Sap. *Plant Physiol.* **119**, 1001–1008 (1999).

60. S. Kumar, G. Stecher, M. Li, C. Knyaz, K. Tamura, MEGA X: Molecular evolutionary genetics analysis across computing platforms. *Mol. Biol. Evol.* **35**, 1547–1549 (2018).

61. Z. Dong *et al.*, Maize LAZY1 mediates shoot gravitropism and inflorescence development through regulating auxin transport, auxin signaling, and light response. *Plant Physiol.* **163**, 1306–1322 (2013).

62. G. Chuck, C. Whipple, D. Jackson, S. Hake, The maize SBP-box transcription factor encoded by tasselsheath4 regulates bract development and the establishment of meristem boundaries. *Development* **137**, 1243–1250 (2010).

63. Z. Dong *et al.*, Ideal crop plant architecture is mediated by *tassels replace upper ears1*, a BTB/POZ ankyrin repeat gene directly targeted by TEOSINTE BRANCHED1. *Proc. Natl. Acad. Sci. U.S.A.* **114**, E8656–E8664 (2017).

64. A. Bartlett *et al.*, Mapping genome-wide transcription-factor binding sites using DAP-seq. *Nat. Protoc.* **12**, 1659–1672 (2017).

65. Y. Guo, S. Mahony, D. K. Gifford, High resolution genome wide binding event finding and motif discovery reveals transcription factor spatial binding constraints. *PLOS Comput. Biol.* **8**, e1002638 (2012).

66. J. T. Robinson *et al.*, Integrative genomics viewer. *Nat. Biotechnol.* **29**, 24–26 (2011).

67. P. Machanick, T. L. Bailey, MEME-ChIP: Motif analysis of large DNA datasets. *Bioinformatics* **27**, 1696–1697 (2011).

68. A. Dobin *et al.*, STAR: Ultrafast universal RNA-seq aligner. *Bioinformatics* **29**, 15–21 (2013).

69. M. D. Robinson, D. J. McCarthy, G. K. Smyth, edgeR: A Bioconductor package for differential expression analysis of digital gene expression data. *Bioinformatics* **26**, 139–140 (2010).

70. D. J. McCarthy, Y. Chen, G. K. Smyth, Differential expression analysis of multifactor RNA-seq experiments with respect to biological variation. *Nucleic Acids Res.* **40**, 4288–4297 (2012).

PLANT BIOLOGY

Dong et al.

www.manaraa.com